
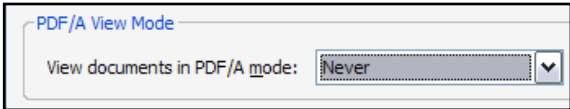
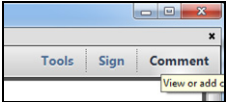
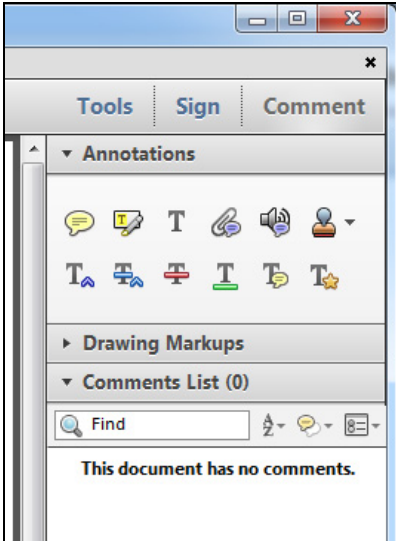


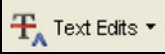


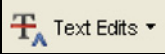

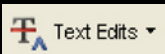





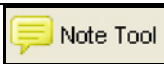

## INSTRUCTIONS ON THE ANNOTATION OF PDF FILES

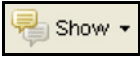
To view, print and annotate your article you will need Adobe Reader version 9 (or higher). This program is freely available for a whole series of platforms that include PC, Mac, and UNIX and can be downloaded from <http://get.adobe.com/reader/>. The exact system requirements are given at the Adobe site: <http://www.adobe.com/products/reader/tech-specs.html>.

*Note: if you opt to annotate the file with software other than Adobe Reader then please also highlight the appropriate place in the PDF file.*

PDF ANNOTATIONS	
Adobe Reader version 9	Adobe Reader version X and XI
<p>When you open the PDF file using Adobe Reader, the Commenting tool bar should be displayed automatically; if not, click on 'Tools', select 'Comment &amp; Markup', then click on 'Show Comment &amp; Markup tool bar' (or 'Show Commenting bar' on the Mac). If these options are not available in your Adobe Reader menus then it is possible that your Adobe Acrobat version is lower than 9 or the PDF has not been prepared properly.</p>  <p>(Mac)</p> <p><b>PDF ANNOTATIONS (Adobe Reader version 9)</b></p> <p>The default for the Commenting tool bar is set to 'off' in version 9. To change this setting select 'Edit   Preferences', then 'Documents' (at left under 'Categories'), then select the option 'Never' for 'PDF/A View Mode'.</p>  <p>(Changing the default setting, Adobe version 9)</p>	<p>To make annotations in the PDF file, open the PDF file using Adobe Reader XI, click on 'Comment'.</p> <p>If this option is not available in your Adobe Reader menus then it is possible that your Adobe Acrobat version is lower than XI or the PDF has not been prepared properly.</p>  <p>This opens a task pane and, below that, a list of all Comments in the text. These comments initially show all the changes made by our copyeditor to your file.</p> 

**HOW TO...**

Action	Adobe Reader version 9	Adobe Reader version X and XI
<b>Insert text</b>	Click the 'Text Edits' button  on the Commenting tool bar. Click to set the cursor location in the text and simply start typing. The text will appear in a commenting box. You may also cut-and-paste text from another file into the commenting box. Close the box by clicking on 'x' in the top right-hand corner.	Click the 'Insert Text' icon  on the Comment tool bar. Click to set the cursor location in the text and simply start typing. The text will appear in a commenting box. You may also cut-and-paste text from another file into the commenting box. Close the box by clicking on 'x'  in the top right-hand corner.
<b>Replace text</b>	Click the 'Text Edits' button  on the Commenting tool bar. To highlight the text to be replaced, click and drag the cursor over the text. Then simply type in the replacement text. The replacement text will appear in a commenting box. You may also cut-and-paste text from another file into this box. To replace formatted text (an equation for example) please <a href="#">Attach a file</a> (see below).	Click the 'Replace (Ins)' icon  on the Comment tool bar. To highlight the text to be replaced, click and drag the cursor over the text. Then simply type in the replacement text. The replacement text will appear in a commenting box. You may also cut-and-paste text from another file into this box. To replace formatted text (an equation for example) please <a href="#">Attach a file</a> (see below).
<b>Remove text</b>	Click the 'Text Edits' button  on the Commenting tool bar. Click and drag over the text to be deleted. Then press the delete button on your keyboard. The text to be deleted will then be struck through.	Click the 'Strikethrough (Del)' icon  on the Comment tool bar. Click and drag over the text to be deleted. Then press the delete button on your keyboard. The text to be deleted will then be struck through.
<b>Highlight text/ make a comment</b>	Click on the 'Highlight' button  on the Commenting tool bar. Click and drag over the text. To make a comment, double click on the highlighted text and simply start typing.	Click on the 'Highlight Text' icon  on the Comment tool bar. Click and drag over the text. To make a comment, double click on the highlighted text and simply start typing.
<b>Attach a file</b>	Click on the 'Attach a File' button  on the Commenting tool bar. Click on the figure, table or formatted text to be replaced. A window will automatically open allowing you to attach the file. To make a comment, go to 'General' in the 'Properties' window, and then 'Description'. A graphic will appear in the PDF file indicating the insertion of a file.	Click on the 'Attach File' icon  on the Comment tool bar. Click on the figure, table or formatted text to be replaced. A window will automatically open allowing you to attach the file. A graphic will appear indicating the insertion of a file.
<b>Leave a note/ comment</b>	Click on the 'Note Tool' button  on the Commenting tool bar. Click to set the location of the note on the document and simply start typing. <u>Do not use this feature to make text edits.</u>	Click on the 'Add Sticky Note' icon  on the Comment tool bar. Click to set the location of the note on the document and simply start typing. <u>Do not use this feature to make text edits.</u>

HOW TO...		
Action	Adobe Reader version 9	Adobe Reader version X and XI
<b>Review</b>	To review your changes, click on the 'Show' button  on the Commenting tool bar. Choose 'Show Comments List'. Navigate by clicking on a correction in the list. Alternatively, double click on any mark-up to open the commenting box.	Your changes will appear automatically in a list below the Comment tool bar. Navigate by clicking on a correction in the list. Alternatively, double click on any mark-up to open the commenting box.
<b>Undo/delete change</b>	To undo any changes made, use the right click button on your mouse (for PCs, Ctrl-Click for the Mac). Alternatively click on 'Edit' in the main Adobe menu and then 'Undo'. You can also delete edits using the right click (Ctrl-click on the Mac) and selecting 'Delete'.	To undo any changes made, use the right click button on your mouse (for PCs, Ctrl-Click for the Mac). Alternatively click on 'Edit' in the main Adobe menu and then 'Undo'. You can also delete edits using the right click (Ctrl-click on the Mac) and selecting 'Delete'.

#### SEND YOUR ANNOTATED PDF FILE BACK TO ELSEVIER

Save the annotations to your file and return as instructed by Elsevier. Before returning, please ensure you have answered any questions raised on the Query Form and that you have inserted all corrections: later inclusion of any subsequent corrections cannot be guaranteed.

#### FURTHER POINTS

- Any (grey) halftones (photographs, micrographs, etc.) are best viewed on screen, for which they are optimized, and your local printer may not be able to output the greys correctly.
- If the PDF files contain colour images, and if you do have a local colour printer available, then it will be likely that you will not be able to correctly reproduce the colours on it, as local variations can occur.
- If you print the PDF file attached, and notice some 'non-standard' output, please check if the problem is also present on screen. If the correct printer driver for your printer is not installed on your PC, the printed output will be distorted.

## Theory

# Mathematical Modeling of PDGF-Driven Glioblastoma Reveals Optimized Radiation Dosing Schedules

Kevin Leder,<sup>1,9</sup> Ken Pitter,<sup>2,9</sup> Quincey LaPlant,<sup>2</sup> Dolores Hambarzumyan,<sup>3</sup> Brian D. Ross,<sup>4</sup> Timothy A. Chan,<sup>5</sup> Eric C. Holland,<sup>6,\*</sup> and Franziska Michor<sup>7,8,\*</sup>

<sup>1</sup>Department of Industrial and Systems Engineering, University of Minnesota, Minneapolis, MN 55455, USA

<sup>2</sup>Brain Tumor Center, Department of Cancer Biology and Genetics, Memorial Sloan-Kettering Cancer Center, New York, NY 10065, USA

<sup>3</sup>Departments of Neurosciences and Molecular Medicines, Cleveland, OH 44195, USA

<sup>4</sup>Center for Molecular Imaging and Department of Radiology, University of Michigan, Ann Arbor, MI 48109, USA

<sup>5</sup>Human Oncology and Pathogenesis Program, Memorial Sloan-Kettering Cancer Center, New York, NY 10065, USA

<sup>6</sup>Division of Human Biology, Alvorad Brain Tumor Center, University of Washington, Seattle, WA 98109, USA

<sup>7</sup>Department of Biostatistics and Computational Biology, Dana-Farber Cancer Institute, Boston, MA 02215, USA

<sup>8</sup>Department of Biostatistics, Harvard School of Public Health, Boston, MA 02215, USA

<sup>9</sup>These authors contributed equally to this work

\*Correspondence: [eholland@fhcrc.org](mailto:eholland@fhcrc.org) (E.C.H.), [michor@jimmy.harvard.edu](mailto:michor@jimmy.harvard.edu) (F.M.)

<http://dx.doi.org/10.1016/j.cell.2013.12.029>

## SUMMARY

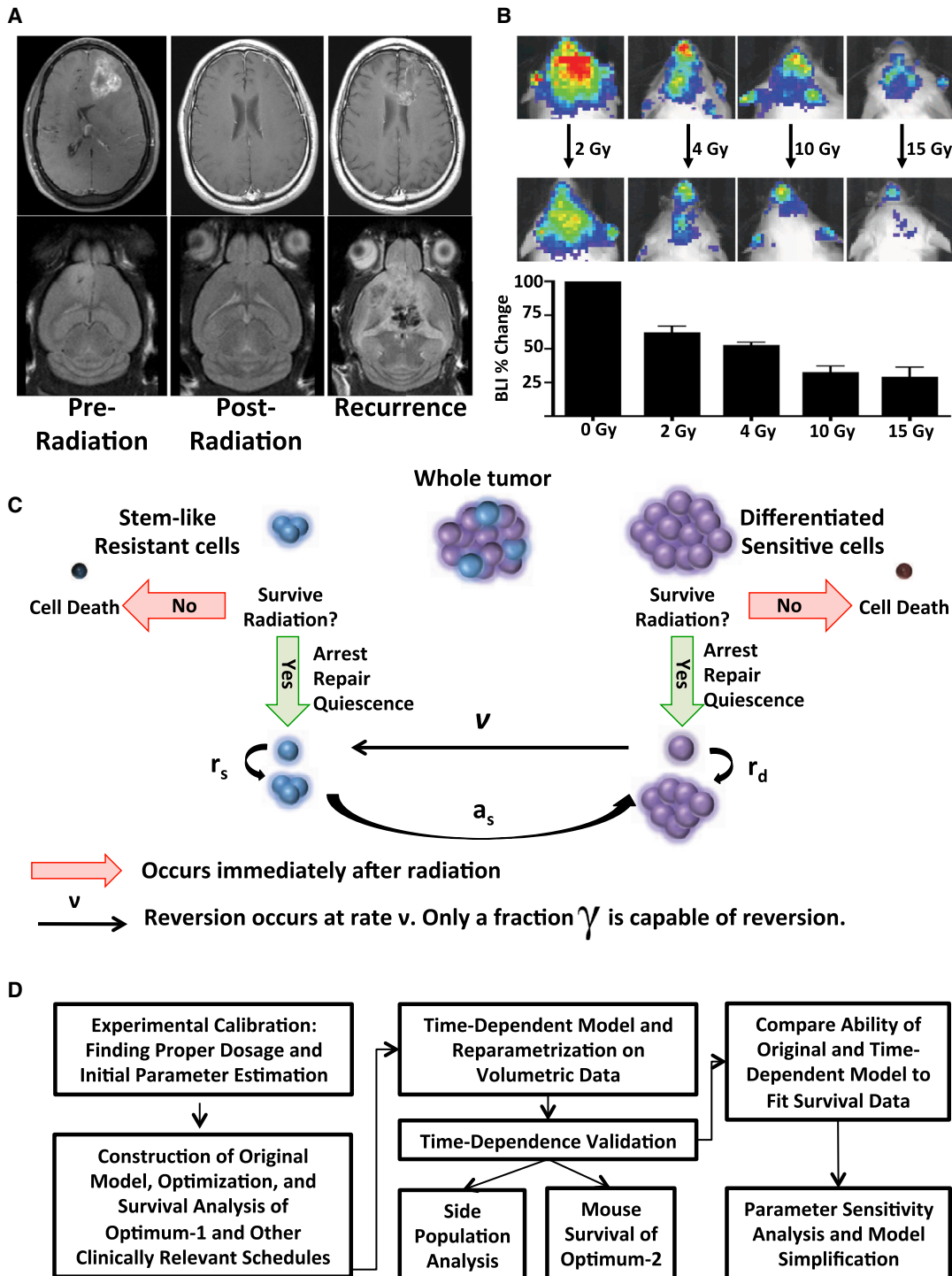
Glioblastomas (GBMs) are the most common and malignant primary brain tumors and are aggressively treated with surgery, chemotherapy, and radiotherapy. Despite this treatment, recurrence is inevitable and survival has improved minimally over the last 50 years. Recent studies have suggested that GBMs exhibit both heterogeneity and instability of differentiation states and varying sensitivities of these states to radiation. Here, we employed an iterative combined theoretical and experimental strategy that takes into account tumor cellular heterogeneity and dynamically acquired radioresistance to predict the effectiveness of different radiation schedules. Using this model, we identified two delivery schedules predicted to significantly improve efficacy by taking advantage of the dynamic instability of radioresistance. These schedules led to superior survival in mice. Our interdisciplinary approach may also be applicable to other human cancer types treated with radiotherapy and, hence, may lay the foundation for significantly increasing the effectiveness of a mainstay of oncologic therapy.

## INTRODUCTION

Patients suffering from glioblastoma (GBM), the most common and malignant primary brain tumor, have very poor survival. The standard of care is surgery when possible followed by radiation (Figure 1A) and chemotherapy (Stupp et al., 2005). This regime has seen little change over the past 50 years, as has the overall survival for this disease. Radiation is used in

adjuvant therapy globally and provides a significant increase in the survival of GBM patients (Walker et al., 1980). Dose escalation studies demonstrated that survival improvements are observed up to an overall dose of 60 Gy (Walker et al., 1979). Beyond this point, there are little, if any, improvements in survival at the cost of increased toxicity (Bleehen and Stenning, 1991; Chan et al., 2002; Morris and Kimple, 2009). Typically, the dosing schedule is 2 Gy per day, 5 days per week, for 6 weeks. Several alternative schedules have been attempted, such as hypofractionated dosing of 3–6 Gy per session, hyperfractionated dosing of 1 Gy fractions two to three times per day, and accelerated dosing using multiple 2 Gy fractions a day to shorten the overall treatment time (Laperriere et al., 2002). None of these strategies, however, have resulted in consistent improvements in tumor control or survival and are thus not routinely used in the clinic.

Three recent advances provide insights into GBM biology that may impact therapy. First is the realization that GBM falls into several molecular subgroups that appear to be dominated by specific signaling pathways (Brennan et al., 2009; Phillips et al., 2006; Verhaak et al., 2010). These subgroups include proneural GBM that is related to abnormal platelet-derived growth factor (PDGF) signaling, classical GBM with canonical epidermal growth factor receptor (*EGFR*) amplification, and mesenchymal GBM with common loss of *NF1* function. The second advance is the development and use of genetically engineered mouse models of GBM that provide genetically and histologically accurate models of these molecular subtypes of GBM (Hambarzumyan et al., 2011; Huse and Holland, 2009; Sharpless and Depinho, 2006). The third development is a series of work describing a subset of glioma cells that share many characteristics with stem cells (Galli et al., 2004; Ignatova et al., 2002; Singh et al., 2004). These cells are preferentially resistant to radiation and temozolomide and are considered an underlying cause of disease recurrence (Bao et al., 2006; Chen et al., 2012; Liu et al., 2006).



**Figure 1. Human and Murine Gliomas Display Similar Recurrence Patterns in Response to Radiation**

(A) Representative MRIs showing human and mouse gliomas that are resolved by radiation treatment but then recur.

(B) Representative images and quantification of a radiation dose response assayed in *E2f1-Luc* glioma-bearing 24 hr after a given radiation dose. Error bars are SD.

(C) Schematic of the mathematical model used to describe the radiation response. The tumor is modeled as two separate cellular components: the stem-like resistant cells (SLRCs) and the differentiated sensitive cells (DSCs). SLRCs can repopulate the tumor, and some DSCs cells, represented by  $\gamma$ , are able to revert to SLRCs in response to radiation.

(D) Flow-chart summarizing the workflow described in the paper.

See also [Figure S1](#).

The PDGF-induced mouse model of GBM accurately mimics the 25%–30% of human GBMs in which aberrant PDGF signaling is present (Brennan et al., 2009; Shih et al., 2004; Verhaak et al., 2010). This model also contains a subpopulation of tumor cells that have similarities to stem cells (Barrett et al., 2012; Bleau et al., 2009; Charles et al., 2010). Stem-like cells are thought to reside in the perivascular niche and are maintained in that state at least partly by nitric oxide (NO) that signals through cyclic guanosine monophosphate, PKG, and NOTCH (Calabrese et al., 2007; Charles et al., 2010; Eyler et al., 2011). Within as little as 2 hr, NO can induce tumor cells to acquire a stem-like phenotype resulting in enhanced neurosphere and tumor formation upon transplantation (Charles et al., 2010). Other niche factors, such as hypoxic conditions, have also been shown to induce stemness (Heddleston et al., 2009; Li et al., 2009). Additionally, recent work has demonstrated that there are multiple tumorigenic cell types within a given tumor and that terminally differentiated astrocytes and neurons can dedifferentiate under oncogenic stress (Chen et al., 2010; Friedmann-Morvinski et al., 2012). These observations suggest that GBMs possess a dynamic heterogeneity of differentiation states that may allow them to rapidly and dynamically acquire a more resistant phenotype.

We hypothesized that mathematical modeling of this dynamic plasticity could be used to enhance radiation therapy. In the past few decades, the vast majority of mathematical modeling of the effects of radiation on cells has been based on the linear quadratic model. This model is widely accepted in the radiation literature due to its close agreement with experimental results for almost all radiation values of clinical interest (Hall and Giaccia, 2012). Several previous studies have specifically investigated the impact of radiotherapy on glioblastoma (Dionysiou et al., 2004; Harpold et al., 2007; Rockne et al., 2009; Stamatakos et al., 2006). These studies range from purely computational experiments to models fitting clinical data and have been utilized in predicting the outcomes of accelerated hyperfractionated schedules. Other recent work has successfully utilized mathematical modeling of cellular in vitro or rat-based in vivo systems to describe glioma behavior (Gao et al., 2013; Massey et al., 2012). Despite the multitude of work that has been done on optimal fractionation schedules, there has been very little success against aggressive gliomas in the clinic (Gupta and Dinshaw, 2005).

Here, we aimed to model a dynamic radiation response with the goal of identifying optimal schedules capable of improving radiation efficacy in a mouse model of PDGF-driven glioma. Our model considers two separate populations of cells: the largely radioresistant stem-like glioma cells and the radiosensitive differentiated glioma cells. We hypothesized that, after exposure to radiation, a fraction of the radiosensitive cells could rapidly revert to the radioresistant state. The inclusion of this dynamic hierarchical population structure and its plasticity induced by exposure to ionizing radiation is a feature of our framework. Based on this model, we described an optimized schedule that was predicted to prolong survival. Crucially, when tested in a clinically relevant glioma mouse model, this schedule markedly improved survival compared to a standard schedule. The fidelity of the model was improved by adding

nonlinear temporal constraints to the acquisition of radioresistant properties based on the time since the previous radiation treatment. This second iteration of the model was able to generate a second optimized schedule that also improved survival in glioma-bearing mice. The mathematical model identifies the fraction of cells capable of acquiring radioresistance and the temporal constraints under which this process occurs as sensitive parameters for predicting radiation response. Specifically, our model predicts that if tumors were unable to rapidly acquire radioresistance, there would be no benefit to any of the optimum schedules. Our data support the functional importance of dynamic radioresistance to therapy and suggests that, at least in PDGF-driven glioma, the standard radiation schedule used may not be optimal. These findings may have broad implications for improving radiation therapy and provide a framework for future optimization of cytotoxic treatment delivery.

## RESULTS

### Initial Characterization of Radiation Dosing Using an Animal Model for PDGF-Driven GBM

We first performed a dose-response study to determine the effectiveness of various single-fraction doses of radiation (Figure 1B). We generated PDGF-B-induced tumors in *Nestin-tv-a;E2f1-Luc* mice using the replication-competent ASLV long-terminal repeat (LTR) with a splice acceptor (RCAS)/*t-va* mouse-model system (Uhrbom et al., 2004). These mice express firefly luciferase driven by the *E2f1* promoter (*E2f1-Luc*), allowing for a noninvasive readout of cellular proliferation. This model is similar to human gliomas, in that glioma-bearing mice transiently respond to radiation treatment but ultimately succumb to disease recurrence (Figure 1A). We irradiated glioma-bearing mice with a variety of single doses: 2 Gy (approximately the daily dose used in humans), 4 Gy, 10 Gy, and 15 Gy. Twenty-four hours after irradiation, we found a progressive decrease in E2F1-driven bioluminescence activity with increasing radiation dose that appeared to plateau around 10 Gy (Figure 1B). For this reason, we chose a 10 Gy dose for further investigations.

### Mathematical Modeling of GBM Cell Dynamics Predicts Treatment Response

We designed a mathematical model of GBM cell dynamics in response to radiation therapy. The model considers two distinct subpopulations of cells: stem-like/resistant cells (SLRCs) and differentiated/sensitive cells (DSCs) (Figure 1C). SLRCs reproduce symmetrically at rate  $r_s$  to give rise to two SLRCs and asymmetrically at rate  $a_s$  to produce a SLRC and a DSC. Initially, the ratio of DSCs to SLRCs is given by  $R$ . Our model incorporates a bidirectional flow of cells between the SLRC and DSC states. In addition to SLRCs converting to a differentiated sensitive state, our model assumes that a fraction of DSCs may be capable of reverting to become SLRCs after exposure to ionizing radiation (Bleau et al., 2009; Charles et al., 2010; Chen et al., 2012; Li et al., 2009; Pistollato et al., 2010). The rate at which DSCs revert to a stem-like state is given by  $\nu$ , and the fraction of DSCs that can revert is given by  $\gamma$ .



SLRCs are relatively radioresistant, whereas DSCs respond to radiation therapy via cell-cycle arrest, mitotic cell death, and apoptosis (Bao et al., 2006; Chen et al., 2012; Hambardzumyan et al., 2008). We modeled the cell-population response to radiotherapy using the linear quadratic model, which is widely accepted in the radiation literature due to its close agreement with experimental results (Dale, 1985; Fowler, 2010). The basic linear quadratic model states that the fraction of cells that survives a radiation dose of  $d$  Gy is given by  $\exp[-\alpha d - \beta d^2]$ . The parameters  $\alpha$  and  $\beta$  are specific to the type of tissue that is being irradiated; the parameter  $\alpha$  represents cell killing resulting from a single radiation track causing damage to a specific chromosomal locus, whereas  $\beta$  represents cell killing via two tracks of radiation causing damage at the same locus. Within our mathematical framework, the parameters  $\alpha_s$  and  $\beta_s$  characterize the response of SLRCs to radiation, whereas the parameters  $\alpha_d$  and  $\beta_d$  denote the response of DSCs. In order to simplify the model, we considered the increased radiosensitivity of DSCs to be expressed in relation to the SLRC radioresistance, represented by the parameter  $\rho$ . In particular, we assumed that  $0 \leq \rho \leq 1$ ,  $\alpha_s = \rho \alpha_d$ , and  $\beta_s = \rho \beta_d$ . Therefore, the sensitivity of SLRCs to radiation can be characterized by a single parameter,  $\rho$ .

Our model also included radiation-induced cell-cycle arrest and attempted DNA-damage repair (Bao et al., 2006). In the context of our model, this arrest lasts for a minimum of  $L_s$  and  $L_d$  time units after radiation exposure in SLRCs and DSCs, respectively, and the rates at which these cells exit cell-cycle arrest are given by  $\lambda_s$  and  $\lambda_d$ . Further, newly converted DSCs take a minimum of  $M_d$  units of time to begin reproducing again, and this event occurs at rate  $\eta_d$ .

Using this notation, we then formulated a mathematical model to describe the numbers of SLRCs and DSCs in response to radiation. At the time of diagnosis of the disease, there are  $N_0^S$  SLRCs and  $N_0^D$  DSCs. When these cells are exposed to the first dose of  $d$  Gy of radiation, there occurs a change in their numbers according to the linear quadratic model, producing  $N_0^S \exp[-\alpha_s d - \beta_s d^2]$  SLRCs and  $N_0^D \exp[-\alpha_d d - \beta_d d^2]$  DSCs. Additionally, there are  $\gamma N_0^D \exp[-\alpha_d d - \beta_d d^2]$  DSCs that are capable of reverting to the SLRC state. Using this description, we can then calculate the number of cells present at time  $t$  after exposure of the population to a dose of radiation. The number of DSCs is given by the number of DSCs that survived radiation and do not have the potential to revert to SLRCs plus any new growth and conversion from SLRCs since treatment; in addition, there are DSCs in the process of reversion. Similarly, the number of SLRCs is given by the population of cells that survived the dose of radiation plus any growth and reversion that has occurred since then:

$$N_1^D = N_0^D e^{-\alpha_d d - \beta_d d^2} \left[ (1 - \gamma) e^{r_d(t-L_d)^+} + \gamma e^{-r_d t} + \alpha_s \gamma \nu \int_0^t e^{r_d(t-s-M_d)^+} \times \int_0^{(s-L_s)^+} e^{-\nu y} e^{r_s(s-y-L_s)^+} dy ds \right] + \alpha_s N_0^S e^{-\alpha_s d - \beta_s d^2} \times \int_{L_s}^{\max(t, L_s)} e^{r_s(s-L_s)} e^{r_d(t-s-M_d)^+} ds,$$

$$N_1^S = N_0^S e^{-\alpha_s d - \beta_s d^2} e^{r_s(t-L_s)^+} + \gamma \nu N_0^D e^{-\alpha_d d - \beta_d d^2} \int_0^t e^{-\nu s} e^{r_s(t-s-L_s)^+} ds$$

where we use the notation  $x^+ = x, x \geq 0$ , and  $x^+ = 0, x < 0$ . Further, note that, for the sake of readability, we have assumed that the rates  $\lambda_s, \lambda_d$ , and  $\eta_d$  are sufficiently large so they can be ignored; for the optimization described below, however, these terms were included (values listed in Table 1). For the full model without this assumption, see Equations 7 and 8 in the Supplemental Information available online.

We can use the analytic description above to predict the response of the tumor to any course of radiation therapy.

### Determination of an Optimal Radiation Schedule

To evaluate the response to a given radiation schedule in the context of our mathematical model, we considered the number of tumor cells present 2 weeks after treatment conclusion as an endpoint. To implement the optimization algorithm, an initial set of parameter values was derived from preliminary data (Figure 1B), previous studies (Galbán et al., 2012; Hambardzumyan et al., 2009; Pitter et al., 2011), or estimates (Table 1; Supplemental Information). We then predicted the survival outcomes for 10 Gy either administered as a single dose or in a clinically standard treatment (5 days of 2 Gy), finding that a standard fractionation schedule would perform significantly better than a single dose (Figures 2A and 2D).

We then aimed to identify an optimal fractionation schedule, with the goal of finding those schedules that minimized the number of tumor cells 2 weeks after the treatment conclusion. Mathematically identifying the global optimal schedule was not computationally feasible due to the complexity of our model, as well as the uncertainty of some of the parameters. Because of this, we utilized simulated annealing, a Monte-Carlo-based method (Kirkpatrick et al., 1983; Van Laarhoven and Aarts, 1987), to identify the best treatment strategies (see Supplemental Information; Table 2).

A clinically motivated constraint set for our schedules is presented in the Supplemental Information. With this constraint set and using our initial set of parameters (Table 1), we identified an optimal schedule, “optimum-1,” that was predicted to do significantly better than standard treatment. We also created a control schedule by generating a scrambled sequence with a similarly clustered dosing scheme that was predicted to not perform significantly better than standard treatment (Figures 2A and 2D; Table 2).

### Optimized Radiation Schedules Significantly Improve Survival in a Mouse Model of PDGF-Driven Glioma

We then returned to the RCAS/*tv*-*va* mouse system to test the model’s predictions in a survival assay. We performed survival experiments using PDGF-B-driven gliomas in *Nestin-tv-a; Ink4a/Arf-/-* mice. The genetic background of these mice is similar to human PDGF-driven tumors (Verhaak et al., 2010). As mice developed symptoms of glioma, such as lethargy, weight loss, seizures, etc., they were randomized into either the mock-treated group or one of the various 10 Gy radiation treatment groups, which consisted of a single dose, standard fractionation, optimum fractionation, and a scramble control

**Table 1. Description and Values of the Mathematical Model Parameters**

Biological Process	Symbol	Original Parameter	Second Iteration	Final Iteration
Per Gy production of lethal DNA lesions from single-radiation track in DSC and SLRC	$\alpha_d/\alpha_s$	0.0987/0.0395	0.0987/0.0429	0.0987/0.00987
Per Gy <sup>2</sup> production of lethal DNA lesions from two radiation tracks in DSC and SLRC	$\beta_d/\beta_s$	$1.14 \times 10^{-7}/4.58 \times 10^{-8}$	$1.14 \times 10^{-7}/4.96 \times 10^{-8}$	$1.14 \times 10^{-7}/1.14 \times 10^{-8}$
Rate at which newly converted DSC lead to clonal expansion (hr)	$\eta_d$	0.5	0.092	0.054
Minimum time for newly converted DSC to being clonal expansion (hr)	$M_d$	24	313.256	366.3
Minimum time DSC and SLRC are in quiescence (hr)	$L_d/L_s$	24/36	461.46/464.99	193.32/477.02
Rate at which DSC and SLRC exit quiescence	$\lambda_d/\lambda_s$	0.5/0.35	.011/.0001	.1/.0328
Proliferation rate of DSC and SLRC after exiting quiescence	$r_d/r_s$	.0088/.0001	.0057/.0001	.0038/.0008
Initial ratio of DSC to SLRC	R	20	20	20
Rate at which SLRC convert to DSC	$a_s$	0.0001	0.0001	0.0019
Rate of reversion of DSC to SLRC	$\nu$	1.15	3.64	0.45
Fraction of DSC capable of reverting to SLRC	$\gamma$	0.15	0.353	0.4
Time to peak reversion after irradiation	$\mu$	-	3.5	3.25
Width of window of reversion	$\sigma^2$	-	2.5548	1.46

(Table 2). The endpoint of survival was defined as the time point at which the animal had to be sacrificed because of excessive tumor burden: greater than 10% weight loss, lethargy, or seizure. Mock-treated mice quickly succumbed to their disease, with a median overall survival of 5 days after the onset of symptoms (Figure 2B). Animals in the single-dose and the clinical-standard groups had respective median survivals of 28.5 and 33 days after the onset of symptoms, which was significantly longer than the mock-treated group ( $p < 0.0001$ ; Figure 2B). Although the median survival of the single-dose-treated animals was shorter than the standard treatment group, there was no significant difference between treatments (hazard ratio [HR] [95% confidence interval (CI)] = 1.619 [0.8450–3.932];  $p$  value = 0.1742; Figures 2D and 2E).

We also analyzed two different mathematically predicted schedules: optimum-1 and the scrambled control sequence (Figures 2A and 2D; Table 2). The median survival of mice treated with the scrambled control schedule was 30 days (Figure 2B), which was not significantly different from the standard schedule (HR [95% CI] = 1.613 [0.7453–4.863];  $p$  value = 0.2346; Figures 2D and 2E). Mice treated with optimum-1 had a median survival of 50 days (Figure 2B), which was significantly longer than the clinical standard schedule (Figures 2D and 2E; HR [95% CI] = 0.3015 [0.04708–0.3760];  $p$  value = 0.001). Due to the increase in median survival observed with the optimized schedule, we next compared the optimized schedule to 2 weeks of clinical standard therapy; in the latter, mice were treated with 20 Gy, delivered in ten fractions given over 12 days, with a 2-day weekend break. The 20 Gy treatment group had a median survival of 53 days (Figure 2B), which was significantly greater than the 10 Gy clinical standard (Figures 2D and 2E; HR [95% CI] = 0.2084 [0.01295–0.1319];  $p < 0.0001$ ), but not significantly different from optimum-1

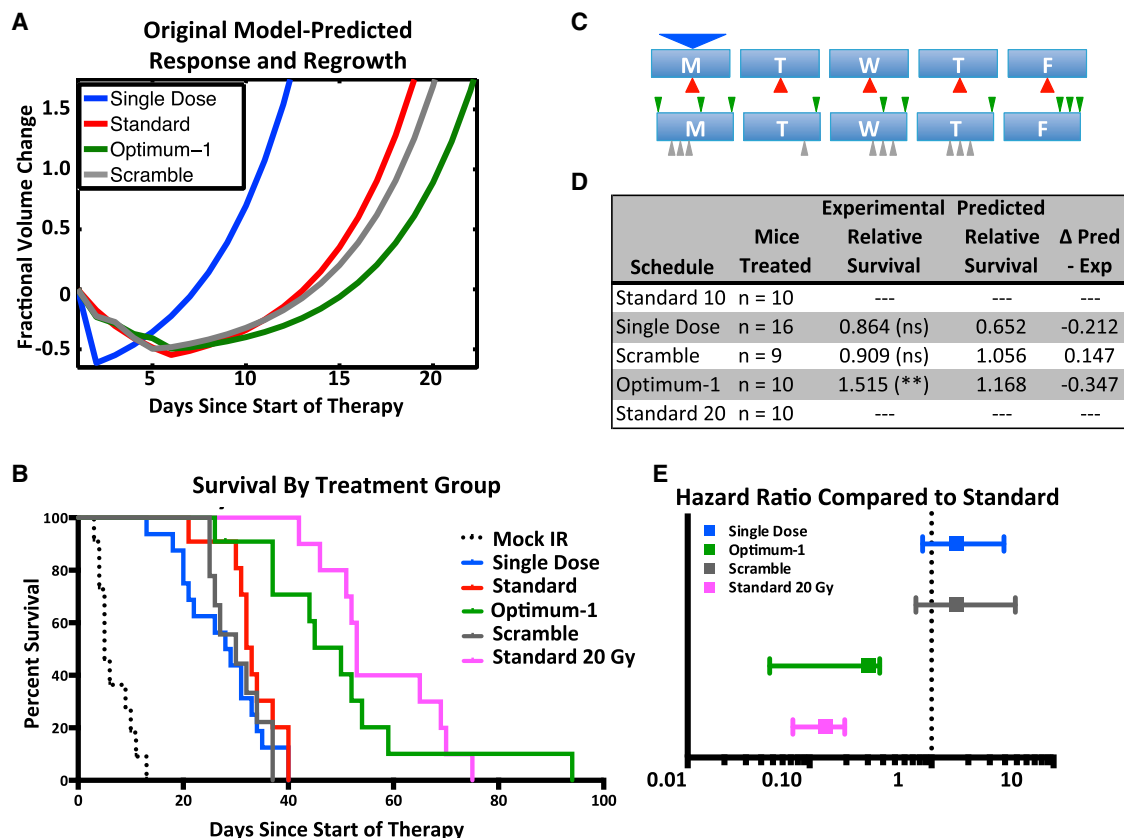
(Figure 2E, HR [95% CI] = 1.429 [0.6230–3.698];  $p$  value = 0.3907).

#### Mathematical Modeling of Other Clinically Relevant Fractionation Schedules Leads to Iterative Updating of the Model

We then set out to investigate other fractionation schedules that have been clinically tested in GBM. Hyperfractionation schedules consist of a large number of smaller-dose treatments in an attempt to minimize damage to surrounding normal tissue, but according to clinical trials, this approach has not improved overall survival (Coughlin et al., 2000; Laperriere et al., 2002). Hypofractionation schedules involve a larger fraction size with fewer treatments, resulting in a shorter overall treatment time that again yields similar survival to conventional therapy (Laperriere et al., 2002). Surprisingly, our initial model predicted that both hypo- and hyperfractionated schedules would perform significantly differently than standard therapy: the hypofractionated schedule was predicted to be similar to a single dose of 10 Gy, whereas a standard hyperfractionated schedule was predicted to perform as well or slightly better than optimum-1 (Figures 3A and 3G).

We tested this prediction for both schedules by overall survival in mice. Mice were randomized as described above into either a hyperfractionated group or hypofractionated group and compared to standard therapy (Table 2). Mice treated with these schedules had a median survival of 37.5 days and 36 days, respectively (Figure 3B). Similar to results observed in human clinical trials, neither of these schedules was significantly different from the clinical standard schedule (Figure 3D; HR<sub>hyper</sub> [95% CI] = 0.5237 [0.1708–1.167];  $p$  value = 0.1383; HR<sub>hypo</sub> [95% CI] = 0.3427 [0.1123–1.046];  $p$  value = 0.0599). These results, and the hyperfractionated schedule in particular, highlighted a





**Figure 2. Mathematical Modeling of the Radiation Response Improves Survival in a Mouse Model of Proneural Glioma**

(A) Original model-predicted tumor response and growth following standard, single-dose, optimum-1, and scramble control radiation treatment schedules. Model parameters are listed under “Original Parameters” in Table 1.

(B) Kaplan-Meier survival plot of various radiation schedules. IR, ionizing radiation.

(C) Schematic depicting the various schedules tested. The arrow position represents the time of dose during the 8am–5pm treatment window. The size of the arrow correlates with the size of the dose.

(D) Table summarizing number of mice treated, the performance relative to standard therapy, and the original model-predicted performance of each group. ns, not significant.

(E) Hazard ratios of the various radiation schedules, compared to the standard radiation schedule. Error bars represent the 95% confidence interval (CI) of the hazard ratio (HR).

See also Figure S2.

weakness in our model that we addressed with a second iteration of the model.

### Time-Dependent Acquisition of Radioresistance Improves the Mathematical Model

To address the inaccurate predictions of the original model, we iteratively updated our model such that the fraction of cells rapidly acquiring resistance,  $\gamma$ , now depends on the time elapsed since the previous dose of radiation. Whereas the initial model treated  $\gamma$  as a time-independent constant following radiation, the updated model stipulates that  $\gamma$  varies over time and that there is a time where a maximum number of cells are prone to reversion in response to subsequent exposure to ionizing radiation. The updated model thus describes the acquisition of resistance with two additional time-dependent parameters: the time of maximal reversion after radiation,  $\mu$ , and the width of the window during which reversion can occur after radiation,

$\sigma^2$ . The model stipulates that, after the first dose of radiation,  $\gamma_0$  cells are capable of reversion; for a later dose given  $t$  hr after the previous dose of radiation, the fraction of cells capable of reversion is given by  $\gamma(t) = \gamma_0 e^{-(t-\mu)^2/\sigma^2}$ . Other than these additional parameters added to further describe  $\gamma$ , the updated model is the same as the original model.

To investigate this time-dependent model, we first tested its predictions against volumetric time series data of mice after treatment with 2 weeks of standard therapy (Figure 3E). This comparison allowed us to identify parameter values capable of recapitulating the time-series data. Based on these model parameters, we found a closer concordance between predicted mouse survival times and observed experimental survival times of the optimum-1, hyperfractionated, hypofractionated, and standard schedules (Figures 3F and 3G). In addition to more accurately predicting the survival response, the model also makes significantly different predictions with regard to the

**Table 2. Description of the Tested Radiation Schedules**

Schedule	Day 1	Day 2	Day 3	Day 4	Day 5
Standard	2 Gy	2 Gy	2 Gy	2 Gy	2 Gy
Single dose	10 Gy	–	–	–	–
Optimum-1	1 Gy	1 Gy	1 Gy	1 Gy	1 Gy-
	8am	5pm	3pm	5pm	3pm
	2pm		5pm		4pm
	5pm				5pm
Scramble control	1 Gy	1 Gy	1 Gy	1 Gy	–
	10am	4pm	2pm	1pm	
	11am		3pm	2pm	
	12pm		4pm	3pm	
Hypofractionated	5 Gy	–	–	–	5 Gy
Hyperfractionated	1 Gy	1 Gy	1 Gy	1 Gy	1 Gy
	9am	9am	9am	9am	9am
	3pm	3pm	3pm	3pm	3pm
Optimum-2	3Gy	1 Gy	–	1 Gy	1 Gy
	8am	4pm		9am	9am
				1pm	1pm
			5pm	5pm	

enrichment of the SLRC population after radiation. Both models similarly predict that 1 day after the last dose, optimum-1 will lead to a larger number of SLRCs relative to standard therapy. However, the models offer differing predictions for the hyperfractionated schedule. The original model predicts that the hyperfractionated schedule maximally enriches the SLRC population among all schedules tested (Figure 4A), whereas the time-dependent model predicts that optimum-1 enriches the SLRC population to a greater extent than the hyperfractionated schedule (Figure 4B).

To test the effects of various schedules on the enrichment of SLRCs, we then treated mice with the standard, hyperfractionated, and optimum-1 schedules. Glioma tissue was harvested for side-population (SP) analysis on the sixth day, i.e., 1 day after the last dose of radiation. Stem-like cells are frequently identified from a variety of normal and malignant tissues by flow cytometry as the SP based their ability to efflux Hoechst dye via the ABC transporter, ABCG2 (Greve et al., 2012). Previous work has demonstrated that, in PDGF-driven murine gliomas, SP cells are enriched for canonical cancer stem cell properties, such as stem-marker expression, enhanced tumor-sphere formation, and enhanced tumorigenicity (Bleau et al., 2009). We generated tumors using a previously described RCAS vector that expresses both PDGF-B and enhanced GFP, which results in gliomas with GFP-positive tumor cells (Fomchenko et al., 2011). This system allowed us to limit the SP analysis to bona fide tumor cells (Figure 4C). We observed that tumors treated with the optimized schedule have a 3.55-fold enrichment when compared to standard therapy (p value = 0.0265; Figure 4D). However, as predicted by the time-dependent mathematical model, the hyperfractionated therapy was able to statistically significantly enrich the SP when compared to standard treatment (1.145-fold enrichment; p value = 0.5944; Figure 4D).

To further validate the time-dependent model, we used this model to derive an optimized schedule, “optimum-2” (Table 2). As with optimum-1, optimum-2 was predicted to lead to an enriched number of SLRCs 1 day after the last dose of radiation compared to standard treatment (Figure 4B). Tumors treated with the optimum-2 schedule had a 2.6-fold enrichment when compared to standard therapy (p value = 0.0210; Figure 4D). Although optimum-2 was predicted to enrich the SLRCs further than optimum-1, we saw no significant difference in the SP between the two groups (p value = 0.3805). We also tested the optimum-2 schedule using overall survival in mice and observed a significant improvement in survival compared to standard treatment (hazard HR [95% CI] 0.2720 [0.04074–0.2967] ratio; p value < 0.0001; Figure 4E). Optimum-2 was also predicted to have significantly longer survival than optimum-1 (Figure S3). The median survival of the optimum-2 group was longer than that of the optimum-1 group; this difference, however, did not reach statistical significance (Figure 4F; HR [95% CI] = 0.8788 [0.4572–1.689], p value = 0.1768).

To further improve the predictive accuracy of the model, we performed a final iteration by reparameterizing the model using the experimental survival data (Figures 5A and 5B). Performing this calculation led to a further confirmation that the time dependence of  $\gamma$  was essential to the model: fitting the time-dependent model to the survival data led to a smaller minimal mean square error as compared to the original model. The time-dependent model was able to fit the observed data to within an error of 5.2 days, in contrast to the original model, which could only fit the data to an error of 16.32 days. Thus, including time-dependent dedifferentiation increases the model's ability to match the survival data. We therefore concluded that the time-dependent form of  $\gamma$  is necessary to accurately explain the observed survival data and it is likely that any cell reversion due to ionizing radiation occurs in a time-dependent fashion.

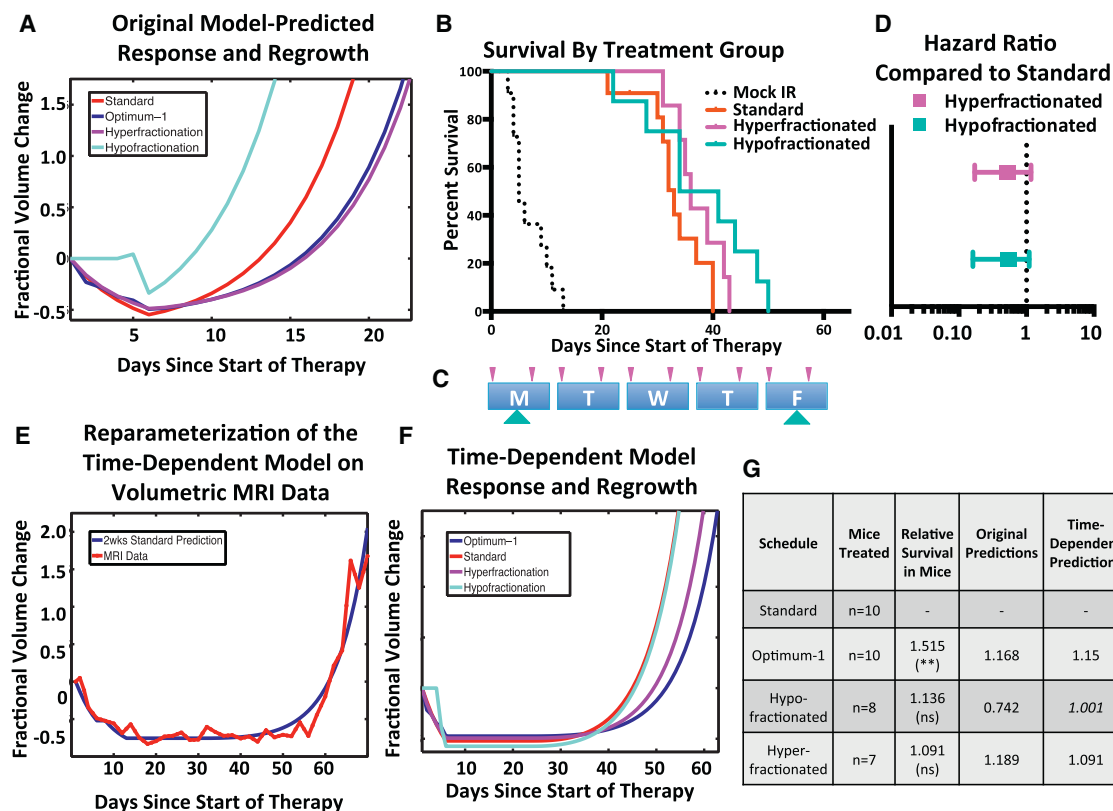
Lastly, we created a simplified version of the model that was more suitable for analysis and interpretation. The simplified model predictions for the tumor cell populations prior to dose  $i+1$  (assuming  $t$  hours between doses  $i$  and  $i+1$ , and  $t_0$  hours between doses  $i-1$  and  $i$ ) are given by

$$N_{i+1}^d = (1 - \gamma(t_0))e^{\gamma_d(t-L_d)} + N_i^d e^{-\alpha_d t}$$

$$N_{i+1}^s = N_i^s e^{-\alpha_s t} + \gamma(t_0)N_i^d e^{-\alpha_d t}$$

According to this simplified form of the model, the optimized therapies optimum-1 and optimum-2 increase survival by converting cells from the fast-growing radiosensitive population to the slow-growing radioresistant population. Notably, sensitivity analysis of the simplified model identifies the parameters that describe reversion as novel sensitivity parameters (Figure 5C; Supplemental Information).

Finally, as a thought experiment, we considered this model in a setting where there is no reversion ( $\gamma_0 = 0$ ) and therefore no ability to rapidly acquire radioresistance. Under these conditions, the model reduces to the standard linear quadratic model, which highlights two important observations. First, in this scenario, all fractionation schedules would result in the same ratio of stem-like to differentiated cells (Figure 5D). This finding is in clear contradiction to the observations of our SP analysis (Figure 4D).



**Figure 3. Comparison of Two Models: Incorporating Dedifferentiation Time Dependence Improves Fidelity**

(A) Predicted tumor growth in response to standard, hypofractionated, hyperfractionated, and optimum-1 radiation treatment schedules. These curves are based on the original model; parameters are listed under Original Parameters in Table 1.

(B) Kaplan-Meier survival plot of hypo- and hyperfractionated radiation schedules. Standard and optimum-1 survival are the same curves as Figure 2 and are shown for comparison.

(C) Schematic depicting the hyper- and hypofractionated schedules tested. The arrow position represents the time of dose during the 8am–5pm treatment window. The size of the arrow correlates with the size of the dose.

(D) Hazard ratios of the hypo- and hyperfractionated radiation schedules, compared to the standard radiation schedule. Error bars represent the 95% CI of the HR.

(E) Reparameterization of the time-dependent model based on volumetric MRI studies of mouse gliomas treated with 2 weeks of the standard schedule.

(F) Time-dependent model-predicted tumor growth in response to the various treatment schedules. Model parameters are listed under “Second Iteration” in Table 1.

(G) Table summarizing number of mice treated, the performance relative to standard therapy, and the predicted performance of the original and time-dependent model for each treatment group.

See also Figure S3.

Second, if there was no reversion, the model predicts all fractionation schedules would result in the same survival (Figure 5E), which is also contradicted by the observations from mouse survival experiments (Figures 2B and 4E). Taken together, these observations provide significant evidence for the fact that ionizing radiation encourages rapid reversion of a subset of glioma cells to a radioresistant stem-like state.

In sum, our iterative mathematical modeling approach, informed and validated by mouse modeling, allowed us to determine not only a radiation delivery schedule that prolonged survival in mice, but also to identify parameters of the biological processes guiding cellular behavior in gliomas that are responsible for radioresistance. This validated mathematical model can be used, in future work, to investigate the effectiveness of alternative schedules and test their effects on GBM cell populations.

## DISCUSSION

Standard radiation delivery schemes are based on decades-old data that mostly predate recent findings on cancer stem cells. In GBM patients, many different radiation schedules have been tried in clinic based on classic radiobiological data, but thus far all have had roughly the same effectiveness. Here, we adopted a combined experimental and theoretical approach with the goal of identifying treatment schedules that would lead to better survival in animal models of the disease by accounting for dynamic transitions of cells between relatively radiosensitive and radioresistant pools. Our approach was based on the assumption that the tumor has a kinetic response to radiation causing some of the surviving cells to acquire resistance by adopting a more stem-like quiescent state over a matter of hours. Based

on this approach, we successfully identified two treatment schedules that significantly extended survival in glioma-bearing mice, whereas a control schedule failed to do so, as predicted. The fact that optimized schedules clearly outperformed other schedules suggests that the response to radiation is dynamic and that the schedule of a given total dose of radiation can affect its ultimate efficacy.

Although the mathematical model presented here offers complexity, it does not include several potentially important biological factors, such as the immune system, stromal-tumor interactions, nutrient gradients, and others. For example, the work by [Stamatikos et al. \(2006\)](#) developed a sophisticated four-dimensional model for the response of high-grade gliomas to ionizing radiation. Based on their computational model, the authors are able to discuss the effects of cell-cycle time, reoxygenation times, and cell density on tumor response to therapy. Whereas these factors are important, using a simplified model focusing on a single factor, such as dynamic radioresistance, is a powerful way to isolate and better study that phenomenon. Additionally, it has previously been shown that working with a simplified model allows for a more thorough exploration of the mathematics behind the specific parameter, which often uncovers nonobvious predictions ([Michor et al., 2005](#); [Norton, 1988](#)). Lastly, simplified models are amenable to more complex mathematical analysis, such as optimization of treatment schedules.

Glioma stem cells are functionally defined by their capacity to self-renew and to generate heterogeneous tumors upon transplantation ([Vescovi et al., 2006](#)). As stem-like cells are more therapeutically resistant and ultimately give rise to recurrent disease, it is commonly believed that decreasing the stem-like population will increase overall survival ([Cheng et al., 2010](#); [Scopelliti et al., 2009](#)). However, our model predicts an improved overall survival for fractionation schedules that enrich the SLRC population. The side population, which is enriched for quiescent stem cells ([Bleau et al., 2009](#); [Deleyrolle et al., 2011](#); [Harris et al., 2008](#)), was elevated in the two optimized schedules that increased overall survival. However, the success of our model is driven by these cells acquiring a quiescent state and slower proliferation rate and therefore is not dependent on a complete dedifferentiation. Further characterization of the ability of radiation to induce other stem-like properties remains an exciting area for future studies.

Whereas eradicating all glioma cells, including the stem-like population, is essential for ultimately curing the disease, our model describes a phenomenon whereby utilizing alternatively fractionated schedules can increase the SLRC population and still result in a slower-growing residual tumor and prolonged time to recurrence. In this regard, our model joins a growing body of evidence suggesting that the relationship between cells with stem-like character and clinical outcomes might not be as straightforward as previously thought. A recent theoretical paper modeling tumor growth kinetics argues that, whereas cancer stem cells are necessary for tumor growth, the kinetics of growth are best described by the nonstem compartment ([Morton et al., 2011](#)). Additionally, a recent human GBM study compared the percentage of CD133+ glioma stem cells in patient-matched primary and recurrent samples ([Pallini et al., 2011](#)). Patients whose gliomas contained an increased percentage of CD133+ at recurrence demonstrated a significantly longer survival than those with decreased CD133+

cells at recurrence. These studies support our finding that a relative enrichment in the resistant stem-like population might prolong survival by increasing the time to recurrence.

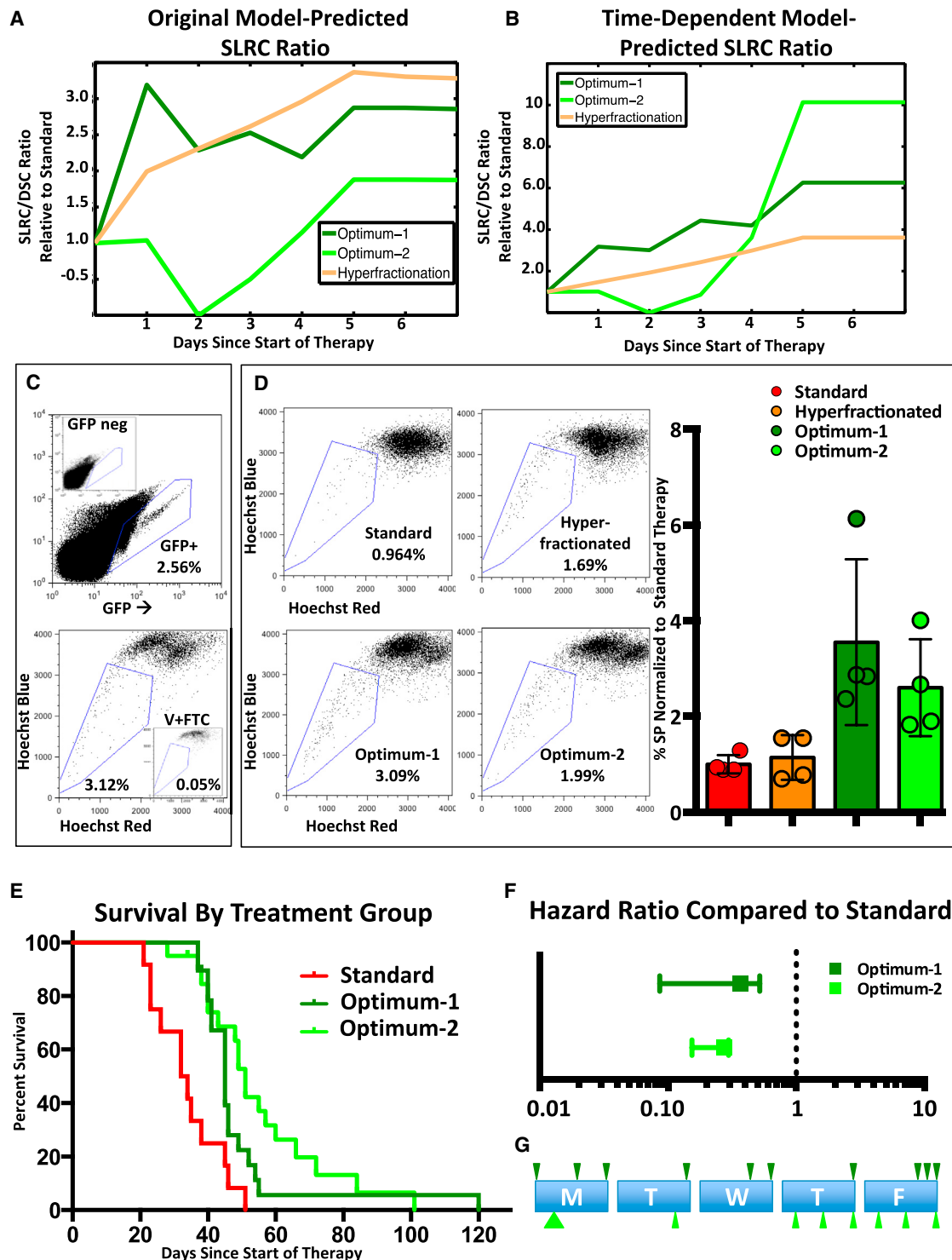
### Translating Optimized Schedules to Human Patients

There are some clear hurdles and open questions in regards to translating our findings from the mouse to the clinic. One measure of predicted toxicity and lethality of different fractionation schedules is given by the biologically effective dose (BED) ([Fowler, 2010](#); [Hall and Giaccia, 2012](#)). This measure is frequently used to compare the effectiveness and toxicity of different schedules. It is difficult to use BED to compare the optimized schedules tested here, as the spacing of our doses is inconsistent. However, if we use the common assumption that doses separated by more than 6 hr are independent, then the optimum-1 schedule had one of the lowest BED values of all schedules tested. Because of this, it might even be possible to increase the dosage levels while keeping the toxicity of the schedule at or below the level of the standard therapy. An important avenue for extending these results to the clinical setting will be to consider optimizing fractionation schedules while stipulating that the schedule has an equal or lower BED than that of standard therapy.

Note also that this treatment approach enriches a slow-growing GSC population and therefore would not be curative. However, previous studies have shown that cancer stem cells are dependent on the NOTCH signaling pathway ([Androuselis-Theotokis et al., 2006](#); [Charles et al., 2010](#); [Eyler et al., 2011](#)), and further studies have shown depletion and therapeutic sensitization of GSCs when treated with gamma-secretase inhibitors ([Gilbert et al., 2010](#); [Hovinga et al., 2010](#); [Wang et al., 2010](#)). Future studies that combine optimized radiation with therapeutics that specifically target GSCs, via NOTCH or other pathways, might further improve outcomes.

GBM is by definition a heterogeneous disease, and it is unclear how robust an optimized schedule developed for proneural glioma would perform across the various other GBM subtypes. The mouse model used in these studies is driven by PDGF signaling, which is characteristic of approximately 25%–30% of human GBMs. Of note, this mouse model might not reflect the biology of other commonly altered signaling pathways, such as *EGFR* amplification or *NF1* loss, and further studies are needed to determine if the optimization will extend to those tumors. Additionally, even tumors with similar molecular underpinnings are likely to exhibit variability in the parameters used to optimize radiation delivery, such as proliferation rate and the fraction of cells capable of rapidly acquiring resistance. This observation brings up the possibility there may be no universal optimum schedule but rather multiple schedules where optimization for a given patient is dependent on detailed pathologic analysis of each resected tumor.

Additionally, the parameter values we used were determined iteratively based on the mouse model, and it is probable that the schedules presented here will not translate precisely to human tumors. Our investigation was performed for 1 week of therapy delivering a total of 10 Gy of radiation. Human patients receive 60 Gy of radiation over 6 weeks, and optimizing that schedule might not simply be six cycles of the 1 week optimized schedules. Nevertheless, our findings suggest that the gliomas



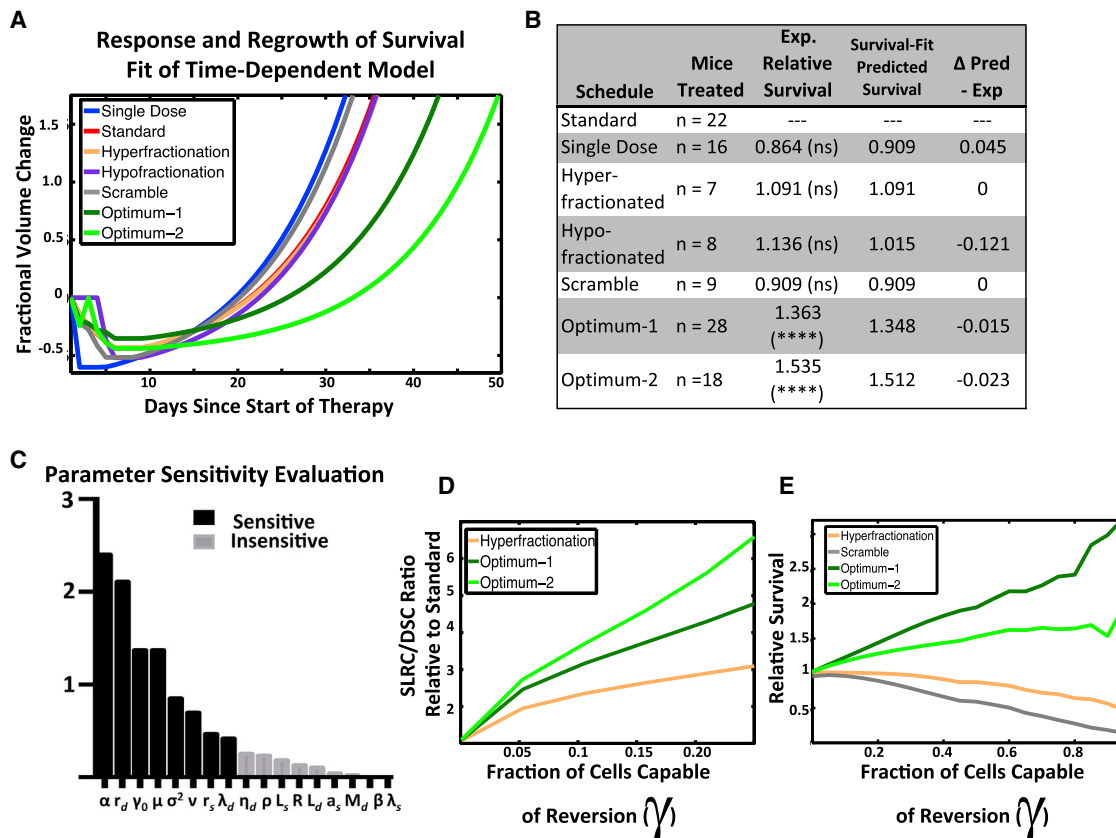
**Figure 4. Optimized Radiation Schedules Enrich the Glioma Stem Cell Population**

(A and B) Graph showing predicted size of the stem-like resistant cell population for hyperfractionated, optimum-1, and optimum-2 schedules, using the original model (A) or the time-dependent model (B). All values are normalized to predictions for standard therapy. Parameters in (A) and (B) are, respectively, from the Original Parameters and Second Iteration in Table 1.

(C) Representative gating strategy for eGFP+ tumor cell side-population (SP) analysis. The upper panel depicts the gate used to identify GFP-positive cells, based on a GFP-negative sample shown in the insert. The lower panel depicts the gate used to identify the SP, based on a Fumitremogin C-verapamil-treated control shown in the insert.

(legend continued on next page)





**Figure 5. Growth Rate and Dynamic Dedifferentiation Are the Most Influential Parameters in Modeling Radiation Response**

(A) Survival-fit, model-predicted tumor growth in response to various radiation treatment schedules. These predictions are from the time-dependent model reparameterized to fit the mouse survival data with the parameters under “Final Iteration” in Table 1.

(B) Table summarizing the number of mice treated, the performance relative to standard therapy, and the predicted performance survival data reparameterized time-dependent model for each treatment group.

(C) Sensitivity analysis of the model’s parameters, ranked from most to least sensitive, as determined by the sensitivity analysis (Supplemental Information).

(D) Predictions of the SLRC/DSC ratio while varying the fraction of cells capable of reversion ( $\gamma_0$ ).

(E) Sensitivity plot showing the relative efficacy of several schedules while varying the fraction of cells capable of reversion ( $\gamma_0$ ). An explanation of how we found the parameters for (E) can be found in Section 5 of the Supplemental Information.

See also Figure S4.

respond dynamically and that the response follows kinetics with a timescale of hours, not weeks. It is therefore imperative to include such considerations into a theoretical framework in order to determine optimum radiation administration schedules for human patients.

Finally, our work studied radiation in isolation, whereas in man, radiation is usually administered after neurosurgical resection and with temozolomide. These treatment modalities need to be incorporated into models aimed at identifying dosing strategies for human patients. Nonetheless, our studies suggest that

modeling glioma response to radiation as a dynamic heterogeneous process can predict a treatment schedule that improves overall survival. It also suggests that the schedule that patients are currently receiving may not be optimal.

## EXPERIMENTAL PROCEDURES

### Generation of Tumors Using RCAS/TVA

All of the animal experiments were conducted using protocols approved by the Institutional Animal Care and Use Committees of Memorial Sloan-Kettering

(D) Representative images and quantification of SP analysis 24 hr after the conclusion of the standard, hyperfractionated, optimum-1, and optimum-2 schedules. For quantification, all values are normalized to the average SP of the standard schedule. Error bars represent the SD.

(E) Kaplan-Meier analysis comparing standard, optimum-1, and optimum-2 schedules. These mice represent an entirely independent cohort from mice in Figures 2 and 3.

(F) Hazard ratios of the optimum-1 and optimum-2, compared to standard radiation.

(G) Schematic briefly describing the optimum-1 and optimum-2 schedules. The arrow position represents the time of dose during the 8am–5pm treatment window. The size of the arrow correlates with the size of the dose. Error bars represent the 95% CI of the HR.

Cancer Center, protocol 00-11-189. Tumors were generated as previously described by injecting RCAS-transfected DF1 cells into *n-tva* mice (Hambardzumyan et al., 2009). Mice were monitored carefully, and treatment began when they displayed neurological symptoms, such as lethargy or head tilt due to tumor burden, at which point they were irradiated for either bioluminescence (BLI) or survival assays. For BLI, mice were analyzed 24 hr after irradiation. For survival, mice were monitored until recurrence of symptoms. The various radiation schedules are described in Table 2; further details on mouse work can be found in the Supplemental Information online.

### MRI Reconstruction and Analysis

Please see the Supplemental Information online.

### SP Analysis

Hoechst 33342 staining was performed as previously reported (Bleau et al., 2009). Briefly, glioma-bearing mice were treated with standard, hyperfractionated, optimum-1, or optimum-2 schedules. Twenty-four hours after the last treatment, mice were euthanized and tissue was harvested for SP analysis. Bona fide tumor cells were identified based on eGFP+ expression, SP was based on Hoescht dye exclusion, and the data were analyzed by FlowJo. Further details on the SP analysis can be found in the Supplemental Information online.

### Statistics

Please see the Supplemental Information online.

### Mathematical Modeling

Please see the Supplemental Information online.

### SUPPLEMENTAL INFORMATION

Supplemental Information includes Extended Experimental Procedures, four figures, and three tables and can be found with this article online at <http://dx.doi.org/10.1016/j.cell.2013.12.029>.

### ACKNOWLEDGMENTS

The authors would like to thank the Holland and Michor labs and Jasmine Foo for discussions and comments and National Institutes of Health grants RO1 CA100688, U54 CA163167, U54 CA143798, U01 CA141502-01 (to E.C.H.), U54 CA143798 (to F.M.), NSF DMS-1224362, U54 CA143798 (to K.L.), MSTP GM07739, F31 NS076028 (to K.P.), and P01 CA085878 (to B.D.R.).

Received: October 10, 2012

Revised: September 18, 2013

Accepted: December 24, 2013

Published: January 30, 2014

### REFERENCES

Androutsellis-Theotokis, A., Leker, R.R., Soldner, F., Hoepfner, D.J., Ravin, R., Poser, S.W., Rueger, M.A., Bae, S.K., Kittappa, R., and McKay, R.D. (2006). Notch signalling regulates stem cell numbers in vitro and in vivo. *Nature* 442, 823–826.

Bao, S., Wu, Q., McLendon, R.E., Hao, Y., Shi, Q., Hjelmeland, A.B., Dewhirst, M.W., Bigner, D.D., and Rich, J.N. (2006). Glioma stem cells promote radioresistance by preferential activation of the DNA damage response. *Nature* 444, 756–760.

Barrett, L.E., Granot, Z., Coker, C., Iavarone, A., Hambardzumyan, D., Holland, E.C., Nam, H.S., and Benezra, R. (2012). Self-renewal does not predict tumor growth potential in mouse models of high-grade glioma. *Cancer Cell* 21, 11–24.

Bleau, A.M., Hambardzumyan, D., Ozawa, T., Fomchenko, E.I., Huse, J.T., Brennan, C.W., and Holland, E.C. (2009). PTEN/PI3K/Akt pathway regulates the side population phenotype and ABCG2 activity in glioma tumor stem-like cells. *Cell Stem Cell* 4, 226–235.

Bleehen, N.M., and Stenning, S.P.; The Medical Research Council Brain Tumour Working Party (1991). A Medical Research Council trial of two radiotherapy doses in the treatment of grades 3 and 4 astrocytoma. *Br. J. Cancer* 64, 769–774.

Brennan, C., Momota, H., Hambardzumyan, D., Ozawa, T., Tandon, A., Pedraza, A., and Holland, E. (2009). Glioblastoma subclasses can be defined by activity among signal transduction pathways and associated genomic alterations. *PLoS ONE* 4, e7752.

Calabrese, C., Poppleton, H., Kocak, M., Hogg, T.L., Fuller, C., Hamner, B., Oh, E.Y., Gaber, M.W., Finklestein, D., Allen, M., et al. (2007). A perivascular niche for brain tumor stem cells. *Cancer Cell* 11, 69–82.

Chan, J.L., Lee, S.W., Fraass, B.A., Normolle, D.P., Greenberg, H.S., Junck, L.R., Gebarski, S.S., and Sandler, H.M. (2002). Survival and failure patterns of high-grade gliomas after three-dimensional conformal radiotherapy. *J. Clin. Oncol.* 20, 1635–1642.

Charles, N., Ozawa, T., Squatrito, M., Bleau, A.M., Brennan, C.W., Hambardzumyan, D., and Holland, E.C. (2010). Perivascular nitric oxide activates notch signaling and promotes stem-like character in PDGF-induced glioma cells. *Cell Stem Cell* 6, 141–152.

Chen, R., Nishimura, M.C., Bumbaca, S.M., Kharbanda, S., Forrest, W.F., Kasman, I.M., Greve, J.M., Soriano, R.H., Gilmour, L.L., Rivers, C.S., et al. (2010). A hierarchy of self-renewing tumor-initiating cell types in glioblastoma. *Cancer Cell* 17, 362–375.

Chen, J., Li, Y., Yu, T.S., McKay, R.M., Burns, D.K., Kernie, S.G., and Parada, L.F. (2012). A restricted cell population propagates glioblastoma growth after chemotherapy. *Nature* 488, 522–526.

Cheng, L., Bao, S., and Rich, J.N. (2010). Potential therapeutic implications of cancer stem cells in glioblastoma. *Biochem. Pharmacol.* 80, 654–665.

Coughlin, C., Scott, C., Langer, C., Coia, L., Curran, W., and Rubin, P. (2000). Phase II, two-arm RTOG trial (94-11) of bischloroethyl-nitrosourea plus accelerated hyperfractionated radiotherapy (64.0 or 70.4 Gy) based on tumor volume (> 20 or < = 20 cm<sup>2</sup>, respectively) in the treatment of newly-diagnosed radiosurgery-ineligible glioblastoma multiforme patients. *Int. J. Radiat. Oncol. Biol. Phys.* 48, 1351–1358.

Dale, R.G. (1985). The application of the linear-quadratic dose-effect equation to fractionated and protracted radiotherapy. *Br. J. Radiol.* 58, 515–528.

Deleyrolle, L.P., Harding, A., Cato, K., Siebzehnrub, F.A., Rahman, M., Azari, H., Olson, S., Gabrielli, B., Osborne, G., Vescevi, A., et al. (2011). Evidence for label-retaining tumour-initiating cells in human glioblastoma. *Brain: a journal of neurology* 134, 1331–1343.

Dionysiou, D.D., Stamatakis, G.S., Uzunoglu, N.K., Nikita, K.S., and Marioli, A. (2004). A four-dimensional simulation model of tumour response to radiotherapy in vivo: parametric validation considering radiosensitivity, genetic profile and fractionation. *J. Theor. Biol.* 230, 1–20.

Eyler, C.E., Wu, Q., Yan, K., MacSwords, J.M., Chandler-Militello, D., Misuraca, K.L., Lathia, J.D., Forrester, M.T., Lee, J., Stamler, J.S., et al. (2011). Glioma stem cell proliferation and tumor growth are promoted by nitric oxide synthase-2. *Cell* 146, 53–66.

Fomchenko, E.I., Dougherty, J.D., Helmy, K.Y., Katz, A.M., Pietras, A., Brennan, C., Huse, J.T., Milosevic, A., and Holland, E.C. (2011). Recruited cells can become transformed and overtake PDGF-induced murine gliomas in vivo during tumor progression. *PLoS ONE* 6, e20605.

Fowler, J.F. (2010). 21 years of biologically effective dose. *Br. J. Radiol.* 83, 554–568.

Friedmann-Morvinski, D., Bushong, E.A., Ke, E., Soda, Y., Marumoto, T., Singer, O., Ellisman, M.H., and Verma, I.M. (2012). Dedifferentiation of neurons and astrocytes by oncogenes can induce gliomas in mice. *Science* 338, 1080–1084.

Galbán, S., Lemasson, B., Williams, T.M., Li, F., Heist, K.A., Johnson, T.D., Leopold, J.S., Chenevert, T.L., Lawrence, T.S., Rehemtulla, A., et al. (2012). DW-MRI as a biomarker to compare therapeutic outcomes in radiotherapy regimens incorporating temozolomide or gemcitabine in glioblastoma. *PLoS ONE* 7, e35857.

- Galli, R., Binda, E., Orfanelli, U., Cipelletti, B., Gritti, A., De Vitis, S., Fiocco, R., Foroni, C., Dimeco, F., and Vescovi, A. (2004). Isolation and characterization of tumorigenic, stem-like neural precursors from human glioblastoma. *Cancer Res.* *64*, 7011–7021.
- Gao, X., McDonald, J.T., Hlatky, L., and Enderling, H. (2013). Acute and fractionated irradiation differentially modulate glioma stem cell division kinetics. *Cancer Res.* *73*, 1481–1490.
- Gilbert, C.A., Daou, M.C., Moser, R.P., and Ross, A.H. (2010). Gamma-secretase inhibitors enhance temozolomide treatment of human gliomas by inhibiting neurosphere repopulation and xenograft recurrence. *Cancer Res.* *70*, 6870–6879.
- Greve, B., Kelsch, R., Spaniol, K., Eich, H.T., and Gotte, M. (2012). Flow cytometry in cancer stem cell analysis and separation. *Cytometry Part A: the journal of the International Society for Analytical Cytology* *81*, 284–293.
- Gupta, T., and Dinshaw, K. (2005). Modified optimal fractionation for poor prognosis malignant gliomas: an elusive search. *Acta Oncol.* *44*, 105–113.
- Hall, E.J., and Giaccia, A.J. (2012). *Radiobiology for the Radiologist* (Philadelphia: Lippincott Williams & Wilkins).
- Hambardzumyan, D., Becher, O.J., Rosenblum, M.K., Pandolfi, P.P., Manova-Todorova, K., and Holland, E.C. (2008). PI3K pathway regulates survival of cancer stem cells residing in the perivascular niche following radiation in medulloblastoma in vivo. *Genes Dev.* *22*, 436–448.
- Hambardzumyan, D., Amankulor, N.M., Helmy, K.Y., Becher, O.J., and Holland, E.C. (2009). Modeling adult gliomas using RCAS/t-va technology. *Transl. Oncol.* *2*, 89–95.
- Hambardzumyan, D., Parada, L.F., Holland, E.C., and Charest, A. (2011). Genetic modeling of gliomas in mice: new tools to tackle old problems. *Glia* *59*, 1155–1168.
- Harpold, H.L., Alvord, E.C., Jr., and Swanson, K.R. (2007). The evolution of mathematical modeling of glioma proliferation and invasion. *J. Neuropathol. Exp. Neurol.* *66*, 1–9.
- Harris, M.A., Yang, H., Low, B.E., Mukherjee, J., Guha, A., Bronson, R.T., Shultz, L.D., Israel, M.A., and Yun, K. (2008). Cancer stem cells are enriched in the side population cells in a mouse model of glioma. *Cancer Res.* *68*, 10051–10059.
- Heddleston, J.M., Li, Z., McLendon, R.E., Hjelmeland, A.B., and Rich, J.N. (2009). The hypoxic microenvironment maintains glioblastoma stem cells and promotes reprogramming towards a cancer stem cell phenotype. *Cell Cycle* *8*, 3274–3284.
- Hovinga, K.E., Shimizu, F., Wang, R., Panagiotakos, G., Van Der Heijden, M., Moayedpardazi, H., Correia, A.S., Soulet, D., Major, T., Menon, J., and Tabar, V. (2010). Inhibition of notch signaling in glioblastoma targets cancer stem cells via an endothelial cell intermediate. *Stem Cells* *28*, 1019–1029.
- Huse, J.T., and Holland, E.C. (2009). Genetically engineered mouse models of brain cancer and the promise of preclinical testing. *Brain Pathol.* *19*, 132–143.
- Ignatova, T.N., Kukekov, V.G., Laywell, E.D., Suslov, O.N., Vrionis, F.D., and Steindler, D.A. (2002). Human cortical glial tumors contain neural stem-like cells expressing astroglial and neuronal markers in vitro. *Glia* *39*, 193–206.
- Kirkpatrick, S., Gelatt, C.D., Jr., and Vecchi, M.P. (1983). Optimization by simulated annealing. *Science* *220*, 671–680.
- Laperriere, N., Zuraw, L., and Cairncross, G.; Cancer Care Ontario Practice Guidelines Initiative Neuro-Oncology Disease Site Group (2002). Radiotherapy for newly diagnosed malignant glioma in adults: a systematic review. *Radiother. Oncol.* *64*, 259–273.
- Li, Z., Bao, S., Wu, Q., Wang, H., Eyler, C., Sathornsumetee, S., Shi, Q., Cao, Y., Lathia, J., McLendon, R.E., et al. (2009). Hypoxia-inducible factors regulate tumorigenic capacity of glioma stem cells. *Cancer Cell* *15*, 501–513.
- Liu, G., Yuan, X., Zeng, Z., Tunici, P., Ng, H., Abdulkadir, I.R., Lu, L., Irvin, D., Black, K.L., and Yu, J.S. (2006). Analysis of gene expression and chemoresistance of CD133+ cancer stem cells in glioblastoma. *Mol. Cancer* *5*, 67.
- Massey, S.C., Assanah, M.C., Lopez, K.A., Canoll, P., and Swanson, K.R. (2012). Glial progenitor cell recruitment drives aggressive glioma growth: mathematical and experimental modelling. *J. R. Soc. Interface* *9*, 1757–1766.
- Michor, F., Hughes, T.P., Iwasa, Y., Branford, S., Shah, N.P., Sawyers, C.L., and Nowak, M.A. (2005). Dynamics of chronic myeloid leukaemia. *Nature* *435*, 1267–1270.
- Morris, D.E., and Kimple, R.J. (2009). Normal tissue tolerance for high-grade gliomas: is it an issue? *Semin. Radiat. Oncol.* *19*, 187–192.
- Morton, C.I., Hlatky, L., Hahnfeldt, P., and Enderling, H. (2011). Non-stem cancer cell kinetics modulate solid tumor progression. *Theor. Biol. Med. Model.* *8*, 48.
- Norton, L. (1988). A Gompertzian model of human breast cancer growth. *Cancer Res.* *48*, 7067–7071.
- Pallini, R., Ricci-Vitiani, L., Montano, N., Mollinari, C., Biffoni, M., Cenci, T., Pierconti, F., Martini, M., De Maria, R., and Larocca, L.M. (2011). Expression of the stem cell marker CD133 in recurrent glioblastoma and its value for prognosis. *Cancer* *117*, 162–174.
- Phillips, H.S., Kharbanda, S., Chen, R., Forrest, W.F., Soriano, R.H., Wu, T.D., Misra, A., Nigro, J.M., Colman, H., Soroceanu, L., et al. (2006). Molecular subclasses of high-grade glioma predict prognosis, delineate a pattern of disease progression, and resemble stages in neurogenesis. *Cancer Cell* *9*, 157–173.
- Pistollato, F., Abbadi, S., Rampazzo, E., Persano, L., Della Puppa, A., Frasson, C., Sarto, E., Scienza, R., D'avella, D., and Basso, G. (2010). Intratumoral hypoxic gradient drives stem cells distribution and MGMT expression in glioblastoma. *Stem Cells* *28*, 851–862.
- Pitter, K.L., Galbán, C.J., Galbán, S., Tehrani, O.S., Li, F., Charles, N., Bradbury, M.S., Becher, O.J., Chenevert, T.L., Rehemtulla, A., et al. (2011). Perifosine and CCI 779 co-operate to induce cell death and decrease proliferation in PTEN-intact and PTEN-deficient PDGF-driven murine glioblastoma. *PLoS ONE* *6*, e14545.
- Rockne, R., Alvord, E.C., Jr., Rockhill, J.K., and Swanson, K.R. (2009). A mathematical model for brain tumor response to radiation therapy. *J. Math. Biol.* *58*, 561–578.
- Scopelliti, A., Cammareri, P., Catalano, V., Saladino, V., Todaro, M., and Stassi, G. (2009). Therapeutic implications of Cancer Initiating Cells. *Expert Opin. Biol. Ther.* *9*, 1005–1016.
- Sharpless, N.E., and Depinho, R.A. (2006). The mighty mouse: genetically engineered mouse models in cancer drug development. *Nat. Rev. Drug Discov.* *5*, 741–754.
- Shih, A.H., Dai, C., Hu, X., Rosenblum, M.K., Koutcher, J.A., and Holland, E.C. (2004). Dose-dependent effects of platelet-derived growth factor-B on glial tumorigenesis. *Cancer Res.* *64*, 4783–4789.
- Singh, S.K., Hawkins, C., Clarke, I.D., Squire, J.A., Bayani, J., Hide, T., Henkelman, R.M., Cusimano, M.D., and Dirks, P.B. (2004). Identification of human brain tumour initiating cells. *Nature* *432*, 396–401.
- Stamatikos, G.S., Antipas, V.P., Uzunoglu, N.K., and Dale, R.G. (2006). A four-dimensional computer simulation model of the in vivo response to radiotherapy of glioblastoma multiforme: studies on the effect of clonogenic cell density. *Br. J. Radiol.* *79*, 389–400.
- Stupp, R., Mason, W.P., van den Bent, M.J., Weller, M., Fisher, B., Taphoorn, M.J., Belanger, K., Brandes, A.A., Marosi, C., Bogdahn, U., et al.; European Organisation for Research and Treatment of Cancer Brain Tumor and Radiotherapy Groups; National Cancer Institute of Canada Clinical Trials Group (2005). Radiotherapy plus concomitant and adjuvant temozolomide for glioblastoma. *N. Engl. J. Med.* *352*, 987–996.
- Uhrbom, L., Nerio, E., and Holland, E.C. (2004). Dissecting tumor maintenance requirements using bioluminescence imaging of cell proliferation in a mouse glioma model. *Nat. Med.* *10*, 1257–1260.
- Van Laarhoven, P.J., and Aarts, E.H. (1987). *Simulated Annealing* (Dordrecht: Kluwer Academic).
- Verhaak, R.G., Hoadley, K.A., Purdom, E., Wang, V., Qi, Y., Wilkerson, M.D., Miller, C.R., Ding, L., Golub, T., Mesirov, J.P., et al.; Cancer Genome Atlas Research Network (2010). Integrated genomic analysis identifies clinically

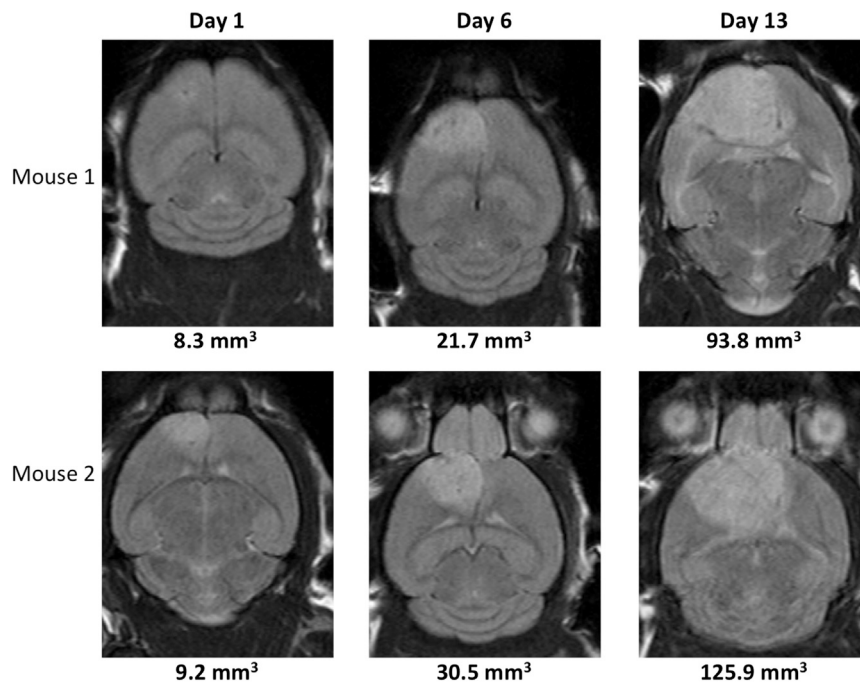
relevant subtypes of glioblastoma characterized by abnormalities in PDGFRA, IDH1, EGFR, and NF1. *Cancer Cell* 17, 98–110.

Vescovi, A.L., Galli, R., and Reynolds, B.A. (2006). Brain tumour stem cells. *Nat. Rev. Cancer* 6, 425–436.

Walker, M.D., Strike, T.A., and Sheline, G.E. (1979). An analysis of dose-effect relationship in the radiotherapy of malignant gliomas. *Int. J. Radiat. Oncol. Biol. Phys.* 5, 1725–1731.

Walker, M.D., Green, S.B., Byar, D.P., Alexander, E., Jr., Batzdorf, U., Brooks, W.H., Hunt, W.E., MacCarty, C.S., Mahaley, M.S., Jr., Mealey, J., Jr., et al. (1980). Randomized comparisons of radiotherapy and nitrosoureas for the treatment of malignant glioma after surgery. *N. Engl. J. Med.* 303, 1323–1329.

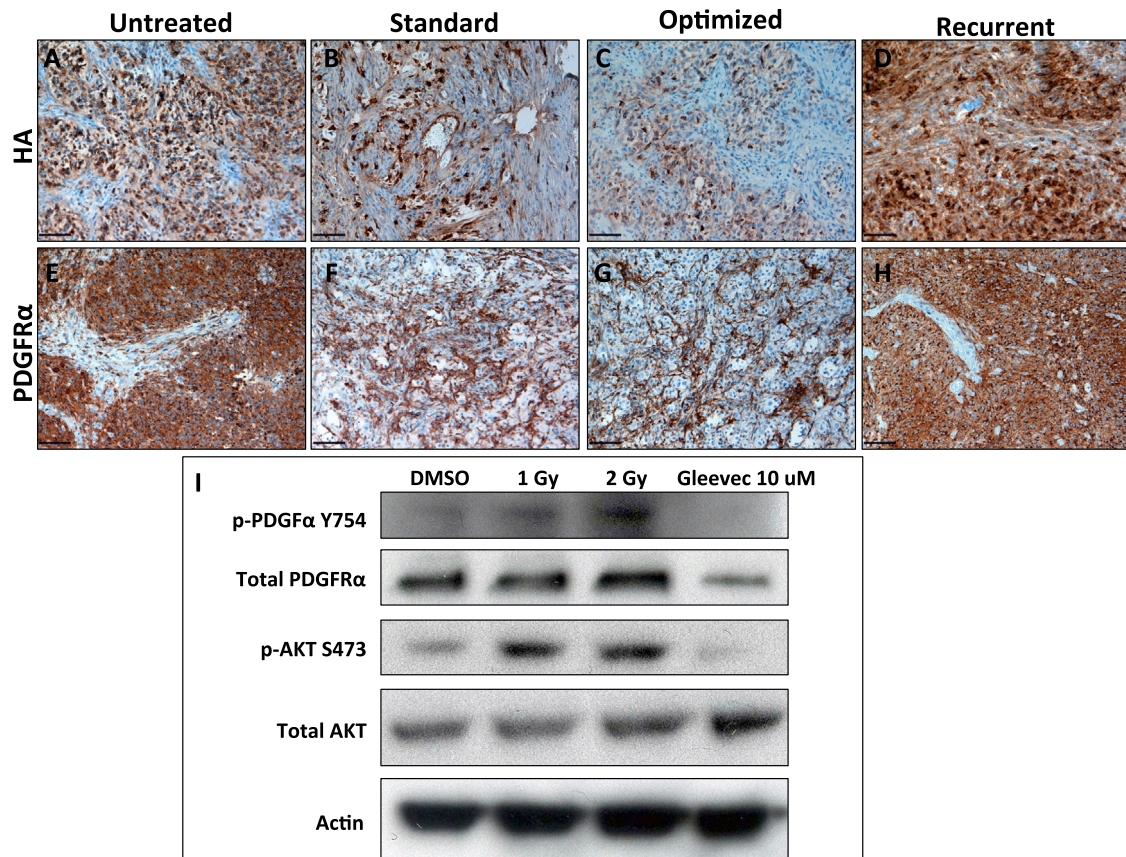
Wang, J., Wakeman, T.P., Lathia, J.D., Hjelmeland, A.B., Wang, X.F., White, R.R., Rich, J.N., and Sullenger, B.A. (2010). Notch promotes radioresistance of glioma stem cells. *Stem Cells* 28, 17–28.



**Figure S1. Growth of Untreated Tumors, Related to Figure 1**

Tumor growth of untreated PDGF-driven gliomas. Glioma bearing mice were monitored by T2-Weighted MRI over the course of 2 weeks to estimate tumor growth. The first day of imaging, day 1, is approximately 1 month after injecting RCAS-PDGFB expressing DF1 cells intracranially.

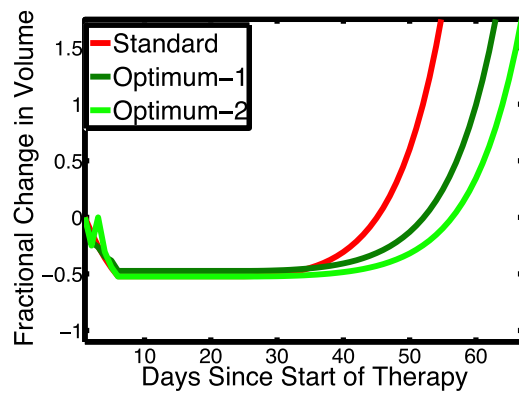




**Figure S2. Radiation Does Not Inhibit PDGF Production or Signaling In Vivo or In Vitro, Related to Figure 2**

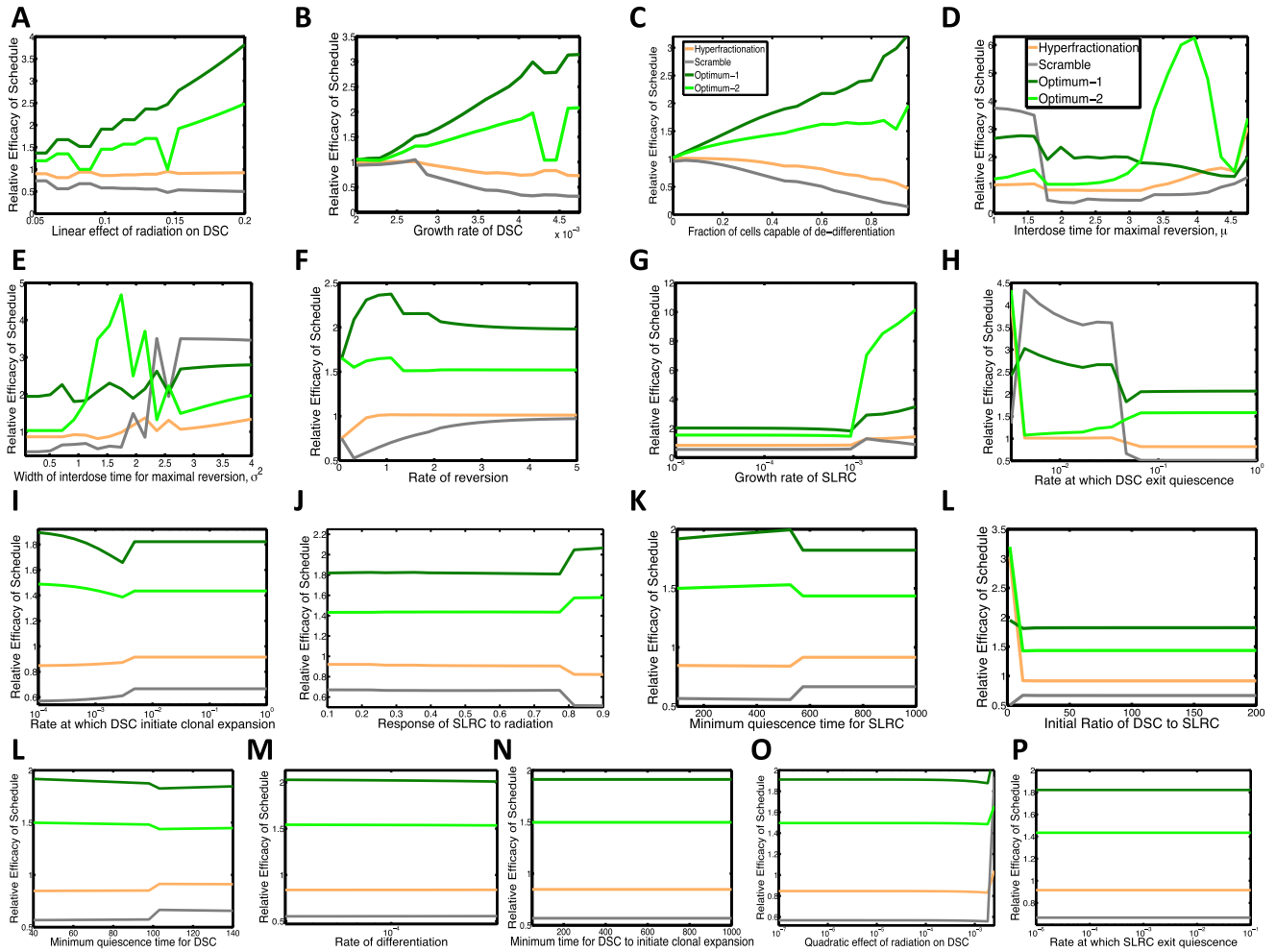
(A-H) Immunohistochemical analysis of PDGF-B ligand (A-D) and PDGF Receptor Alpha (E-H) at either presentation (A,E), one day after conclusion of standard (B,F) or optimum-1 (C,G) treatment, or tumor recurrence (D,H). Staining shows strong expression of both ligand and receptor in untreated tumors. Although radiation treatment decreases the tumor bulk, PDGF-B and PDGFR $\alpha$  positive cells remain, and are sufficient to drive tumor recurrence.

(I) Western blot analysis of a primary mouse glioma cell line treated with radiation or the PDGFR $\alpha$  inhibitor imatinib. Radiation did not inhibit the phosphorylation of PDGFR $\alpha$  or its downstream target AKT, while imatinib was able to inhibit both.



**Figure S3. Time-Dependent Model Predictions, Related to Figure 3**

We plot predicted fractional change in response to the schedules: standard, optimum-1 and optimum-2. These curves are based on the parameter set in the second iteration of the model (see Table 1 of the main text).



**Figure S4. Sensitivity Analysis, Related to Figure 5**

The figure shows the relative efficacy of the hyperfractionated, scramble control, optimum-1, and optimum-2 schedules. To measure relative efficacy, we investigate the ratio of the tumor population under the given schedule to the tumor population under a standard schedule. This comparison is made 60 days after initiation of therapy. In panels (A-P) we vary parameters  $\alpha$ ,  $r_d$ ,  $\sigma^2$ ,  $\mu$ ,  $\nu$ ,  $r_s$ ,  $\lambda_d$ ,  $\eta_d$ ,  $\rho$ ,  $L_s$ ,  $R$ ,  $L_d$ ,  $a_s$ ,  $M_d$ ,  $\beta$  and  $\lambda_s$ , respectively. The parameter  $\gamma_0$  is studied in Figure 5D.